Near-threshold Photoproduction of π^-

A proposal submitted to the 2008 MAX-lab Nuclear Physics PAC
on September 19, 2008

K. G. Fissum, J. Brudvik, K. Hansen, L. Isaksson, M. Lundin, B. Schröder
Lund University and MAX-lab, Sweden

W. Briscoe, R. Hoffman, T. Morrison, M. Paris, I. Strakovsky
The George Washington University, USA

G. V. O'Rielly
University of Massachusetts (Dartmouth), USA

L. S. Myers
University of Illinois, USA

M. F. Taragin
Weizmann Institute of Science, Israel

M. A. Kovash
University of Kentucky, USA

DRAFT

for

The MAX-Tagg Collaboration

1 Motivation

1.1 Introduction to near-threshold pion production

Pion photoproduction at-and-near threshold is a low-energy phenomenon which allows for the formulation and testing of Low-Energy theorems (LETs) [1], QCD-based theories [2], models such as MAID [3] and model-independent technologies such as SAID [4]. Each makes concrete statements about near-threshold pion photoproduction, where the following four reaction channels exist:

$$\gamma + p \rightarrow n + \pi^+ \quad \gamma + n \rightarrow p + \pi^- \quad \gamma + p \rightarrow p + \pi^0 \quad \gamma + n \rightarrow n + \pi^0.$$

At energies close to reaction threshold, the relative angular momentum between the recoiling nucleon and the photopion is predominately s-wave ($l = 0$), with a small p-wave ($l = 1$) component. As this p-wave component is proportional to the momentum of the pion in the center-of-mass frame, it vanishes at threshold while the s-wave component remains finite. Near-threshold measurements of the total photopion production cross section can be extrapolated to threshold, thus providing a direct measurement of the s-wave cross section. This cross section is related to the fundamental Electric Dipole Amplitude E_0^+.

In the past, the magnitude of E_0^+ has been predicted using LETs based on current algebra and partially conserved axial current. Over the past decade, a systematic description of low-energy QCD has been realized. In the energy regime near the pion mass ($m_\pi \sim 140$ MeV/c^2), this description is known as Chiral Perturbation Theory (ChPT). ChPT is an effective field theory in which known symmetries are exploited to restrict the form of possible interactions and thus simplify the calculations. Due to the inclusion of rescattering diagrams in ChPT calculations, these ChPT techniques have resulted in predictions for the threshold amplitudes which differ from the LET predictions.

This difference is most dramatic for the $E_0^+(\pi^0 p)$ and $E_0^+(\pi^0 n)$ amplitudes. In the 1990s, a large amount of beamtime at facilities such as MAMI-B and SAL was thus devoted to the measurements necessary to determine the $E_0^+(\pi^0 p)$ amplitude. Although unresolved normalization problems of 5 – 10% exist between the various data sets, it is by far the most well-investigated of the channels. There are 1188 data points from 10 different data sets spanning the region from threhold to $E_\gamma = 200$ MeV [5]. Unfortunately, followup experiments on the charged pion channels were never performed as the pertinent accelerator facilites were either upgraded in energy or shutdown for retooling. As a result, modern charged pion photoproduction data near threshold are scarce. The bulk of the existing data is at least 20 years old. In fact, only two such measurements have been performed on the charged channels – one each for π^+ [6] and

π^- [7] photoproduction[1]. Table 1 presents a summary of all available charged-pion photoproduction data from threshold to $E_\gamma = 200$ MeV [5], with a focus on the near-threshold post-1990 data from Refs. [6] and [7].

Channel	data points		
	world set [5]	Ref. [6] only	Ref. [7] only
	$E_\gamma < 200$ MeV	$152 < E_\gamma < 154$ MeV	$158 < E_\gamma < 168$ MeV
$\gamma + p \to n + \pi^+$	117	45	0
$\gamma + n \to p + \pi^-$	60	0	12

Table 1
A summary of charged pion photoproduction data sets from threshold to $E_\gamma = 200$ MeV, with a focus on the near-threhold post-1990 data from Refs. [6] and [7]. Note that in order to be effective, models such as MAID and model-independent technologies such as SAID require comparable proton and neutron databases.

This is obviously woefully insufficient, as charged pion photoproduction near threshold is one of few phenomena where both the multipole decomposition and the ChPT predictions converge rapidly. This is because the leading Born terms ensure that the contribution of the pion-loop diagrams is small. Further, while the differences in the ChPT vs. LET predictions are not as dramatic for the charged-photopion channels, ChPT may still be stringently tested. Without these complementary data sets, the comparatively substantial π^0 data cannot be exploited to separate the isospin channels in a model-independent manner, which is important now that predictions based upon the isovectoral pieces of the ChPT Lagrangian are being made, but are by and large unchecked as theory is well ahead of experiment [8]. Finally, it must be noted that to be most effective, models such as MAID and model-independent technologies such as SAID require comparable proton and neutron databases. At present, these databases are not comparable.

1.2 The $E_0^+(\pi^- p)$ amplitude

In general, charged pion production at threshold is well described by the Kroll-Rudermann term [9] which is non-vanishing in the chiral limit. In the limit of massless pions, the LET [1] predicts that the threshold amplitudes for charged pion photoproduction should be equal and opposite to one another, namely $E_0^+(\pi^+ n) = -E_0^+(\pi^- p)$. In the limit of pions with mass, this equality is broken and the LET amplitudes decrease in magnitude. ChPT calculations [2] using the Born, pion, and kaon loops together with ρ-meson

[1] The π^- measurement was performed at TRIUMF using the inverse capture reaction. The status of these data is preliminary – see Sect. 1.3.

exchange produce results that are very similar to those predicted by the LET. In either case, the exact values of the amplitudes depend upon the πNN coupling constant $g^2/4\pi$. Results shown in Table 2 have been determined using two different values for this constant. The first column shows the results originally extracted by the respective authors (using the KH πN PWA result $g^2/4\pi = 14.28$ [10]). The second column shows these results scaled using a constant resulting from a more recent work (the SAID πN PWA result $g^2/4\pi = 13.76$ [11]). We note that most published determinations of the s-wave multipoles for charged pion photoproduction [12,13] are more or less consistent with the LET / ChPT values, with one puzzling exception (see Sect. 1.3).

	$E_0^+(\pi^- p)$ $(\cdot 10^{-3}/m_\pi)$	$E_0^+(\pi^- p)$ $(\cdot 10^{-3}/m_\pi)$
LET	-31.7	-31.1
ChPT	-32.7 ± 0.6	-32.1 ± 0.6
(ChPT : LET)	1.03	1.03

Table 2
LET and ChPT calculations of the $E_0^+(\pi^- p)$ amplitude. The ChPT calculations used the Born, pion, and kaon loops, together with ρ-meson exchange. Values reported in the first column were determined using $g^2/4\pi = 14.28$, while values reported in the second column are the first-column values scaled using $g^2/4\pi = 13.76$.

If we restrict ourselves to the recent SAID energy-dependent FA07 analysis (which is associated with $g^2/4\pi = 13.76$) and the MAID07 analysis [2], the results presented in Table 3 arise.

	$E_0^+(\pi^- p)$ $(\cdot 10^{-3}/m_\pi)$	$E_0^+(\pi^- p)$ $(\cdot 10^{-3}/m_\pi)$
FA07	-31.57	-30.65
MAID07	-30.26	–
(MAID07 : FA07)	0.96	–

Table 3
FA07 and MAID07 predictions for the $E_0^+(\pi^- p)$ amplitude. The value reported in the first column corresponds to the full analysis, while the value reported in the second column corresponds to the Born term only.

The value shown in the first column is for the full analysis, while the value shown in the second column is for the Born term only. The ratio (FA07 : FA07 Born) is 1.03, while the ratio (FA07 : ChPT) is 0.98. The ratio (MAID07 : ChPT) is 0.94.

[2] Some of the disagreement between the SAID and MAID results will always be due to the different parametrizations and databases which are used.

As there are no available data in the near-threshold region, constraint is difficult to provide, and the SAID Single-Energy Solution (SES) and MAID07 Lowest-Energy Solution (LES) are not possible to evaluate until about 40 MeV above threshold. These evaluations are presented in Table 4. While it is impossible to address the uncertainties in the full data-set evaluations, it is possible to address the uncertainties in these limited data-set evaluations, and thus they are very important. Obviously, the fact that restricted data sets are only available 40 MeV above threshold is a concern.

	E_γ (MeV)	$E_0^+(\pi^- p)$ $(\cdot 10^{-3}/m_\pi)$
SAID SES	192	-25.50 ± 1.11
MAID07 LES	190	-26.2 ± 0.4

Table 4
SAID SES and MAID07 LES for the $E_0^+(\pi^- p)$ amplitude. As there are no data in the vicinity of threshold, these solutions are evaluated some 40 MeV above threshold.

1.3 Existing data for π^- photoproduction

Figure 1 shows existing data [7] for the $\gamma + n \rightarrow p + \pi^-$ reaction in the energy region between threshold and 175 MeV. Systematic uncertainties are not shown, but are claimed to be 5%. The data are preliminary. Also shown are the FA07 results (solid blue lines) and MAID07 results (dot-dashed magenta lines). While some discrepancy exists between the two solutions at the backward angles, the overall agreement between both the solutions and the data is very reasonable.

Total cross-section data have been extracted from these results using the Legendre-coefficient extension and are presented in Fig. 2. Total uncertainties are shown. The data are preliminary. Also shown are the FA07 results (solid blue lines) and MAID07 results (dot-dashed magenta lines). Again, the agreement is reasonable.

When these data are used to extract the threshold amplitude $E_0^+(\pi^- p)$, the result is $(-34.6 \pm 1.0) \cdot 10^{-3}/m_\pi$ [7], which is a sizeable deviation from the results of other analyses. We suggest that these data simply lie too far from threshold, and that the p-wave influence is not well-enough understood for a reliable extraction. More precision data near threshold are thus required.

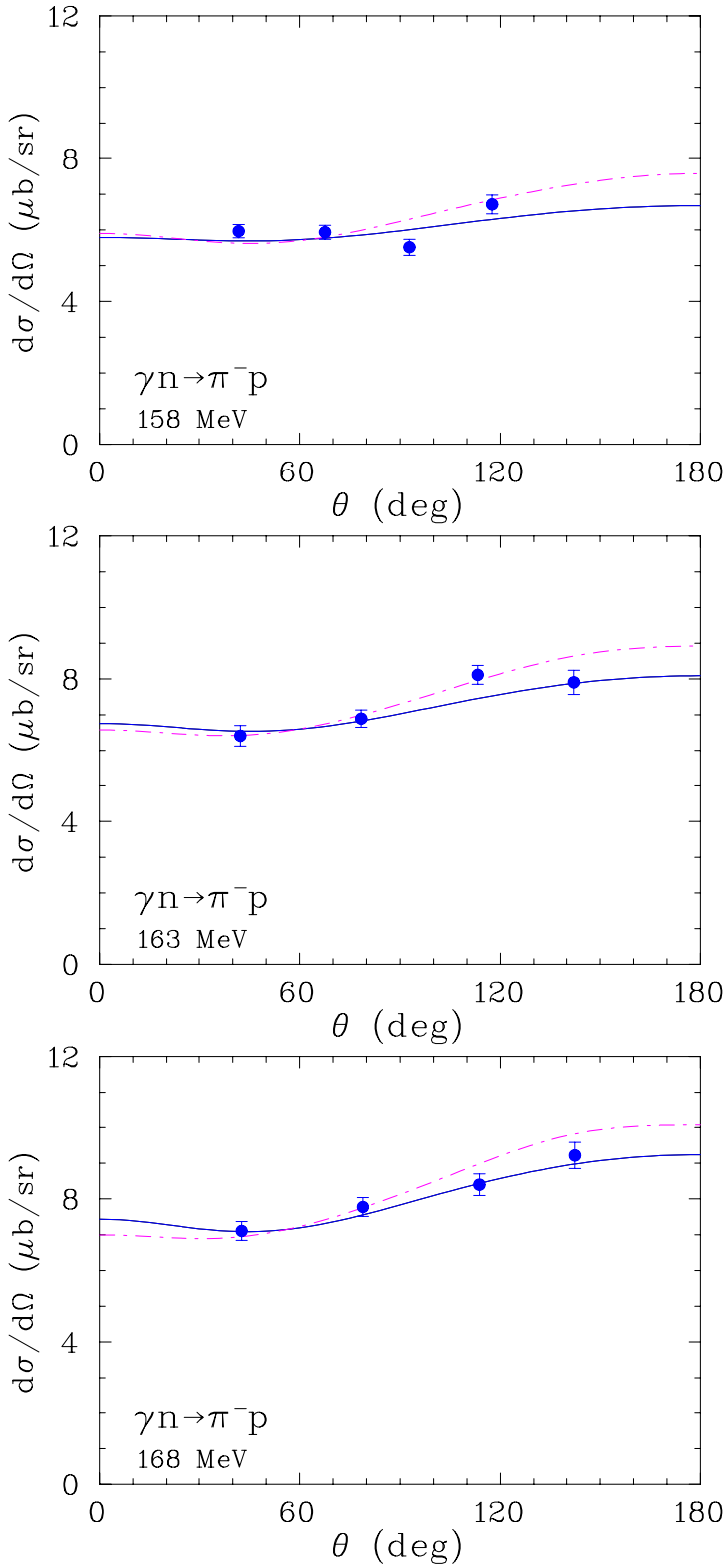

Fig. 1. Existing differential cross-section data for the $\gamma + n \rightarrow p + \pi^-$ reaction for photon energies of 158 MeV (top panel), 163 MeV (middle panel), and 168 MeV (bottom panel). Systematic uncertainties are not shown, but are claimed to be 5%. The data are preliminary. FA07 results are shown by the solid blue lines, while the MAID07 results are shown by the dot-dashed magneta lines.

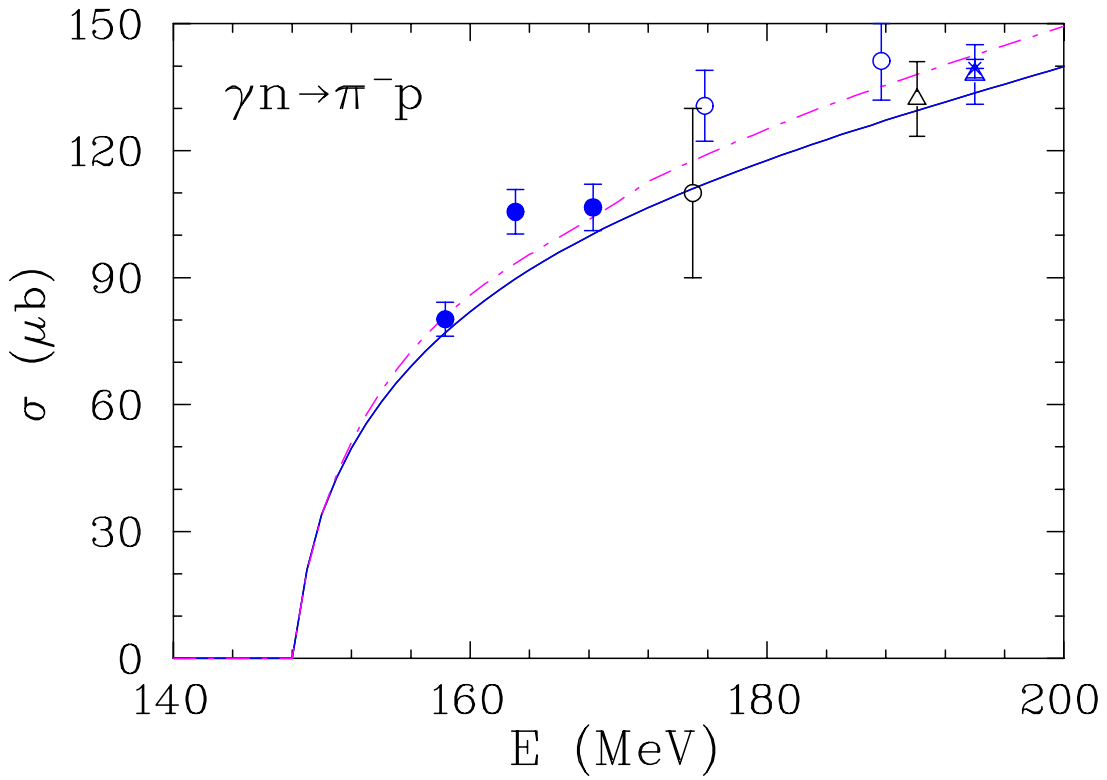

Fig. 2. Existing total cross-section data for the $\gamma + n \rightarrow p + \pi^-$ reaction as a function of photon energy. The data are due to the integration of the differential cross-section data presented in Fig. 1 using a Legendre-coefficient extension. Total uncertainties are shown. The data are preliminary. The FA07 result is shown by the solid blue line, while the MAID07 result is shown by the dot-dashed magneta line.

2 Proposed experiment

2.1 Experimental method – identifying π^-s

In π^0 or π^+ photoproduction measurements, pions may be indentified by their decay products. In the case of π^- photoproduction, this is not possible, since most of the π^-s are captured before they can decay. Instead, we intend to investigate the fundamental $\gamma + n \rightarrow p + \pi^-$ process using a deuterium target via a "two-step" process. The second step in the process involves the capture of the photoproduced π^-s in the target deuterium. This capture leads to the following dominant reactions:

$$\pi^- + d \rightarrow 2n \ (\sim 75\%) \qquad \pi^- + d \rightarrow 2n + \gamma \ (\sim 25\%)\,[3]\,.$$

In the case of the first reaction (which occurs approximately 75% of the time), the two neutrons resulting from the capture of the π^- are emitted with a definite energy

[3] The reaction $\pi^- + d \rightarrow 2n + \pi^0$ is also in principle possible, but is greatly suppressed by parity. The branching ratio is <0.1%, and thus it is not feasible to measure.

(68 MeV) and an isotropic angular distribution. In order to detect these neutrons, a large acceptance neutron detector is required. For the remainder of this proposal, we shall refer to this reaction as the "neutron channel". In the case of the second reaction (which occurs approximately 25% of the time), the two neutrons are emitted very close to one another so that two-body kinematics are approximated. This results in an almost monochromatic capture-photon distribution peaked near 128 MeV (endpoint energy 131.4 MeV) – see Fig. 3. Here, large-volume photon detectors are required. For the remainder of this proposal, we shall refer to this reaction as the "photon channel".

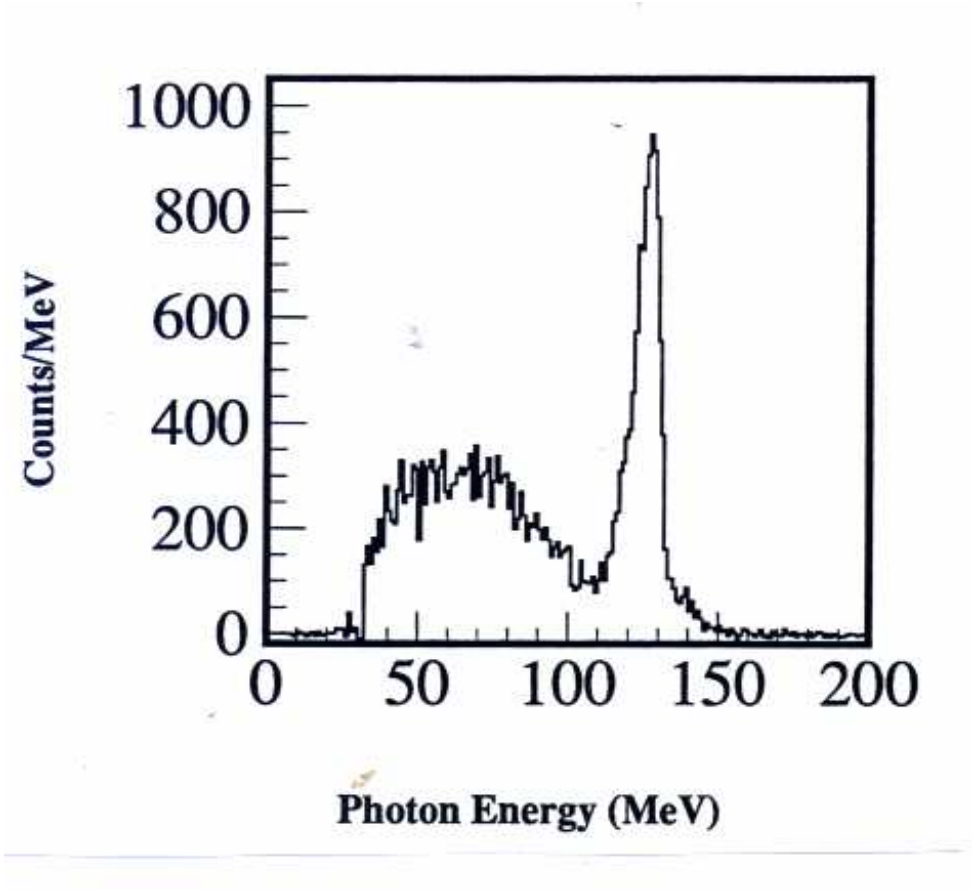

Fig. 3. Gamma-ray spectrum obtained using the BUNI NaI (see Sect. 2.2.3) detector together with the SAL main photon tagger obtained in a test measurement of the photon channel in the mid 1990s at SAL [14]. The tagged photon energy range was 130 to 162 MeV. Backgrounds measured by filling the target cell with liquid hydrogen have been removed – see Sec. 2.3.4 for our discussion of backgrounds. The sharp predominant peak at 130 MeV is due to the radiative capture of π^-s by the target deuterium. While the data were never analyzed to completion, we note that both the tagger and BUNI are now at MAX-lab and ready to be used to complete the project they were used to initiate over a decade ago.

In this experiment, we intend to measure both the neutron and the photon channels simultaneously in order to better understand our systematics.

2.2 Equipment

2.2.1 Beam and tagger

We intend to employ a nominal electron-beam energy of 194 MeV. We will use the 300 μm Al radiator and detect the post-bremsstrahlung electrons using the ET (end-point tagger) [15] operated at 130 A (0.2 T) together with the SAL focal plane [16] (see Fig. 4) placed at a location of 145 mm from the so-called "reference point A" and operated in 100% overlap mode [4].

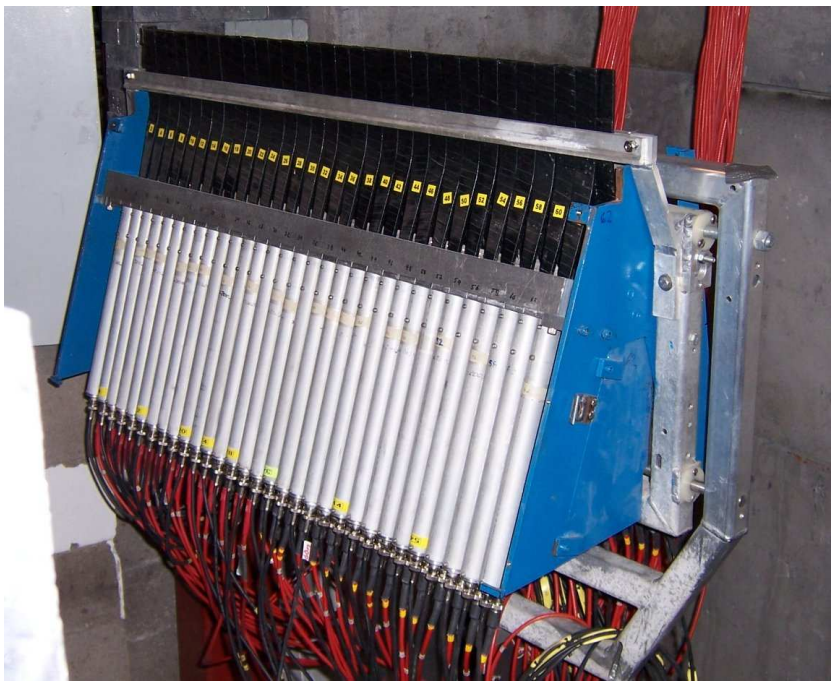

Fig. 4. The SAL focal plane. A 100% overlap mode will be employed resulting in a 32-channel tagged-photon "bite" from 146 – 167 MeV, or roughly 650 keV per channel.

This will result in a tagged-photon "bite" from 146 – 167 MeV, or roughly 650 keV per channel for each of the 32 channels. The photon beam will be collimated using a 25 mm collimator (see Sect. 2.3.2), resulting in a tagging efficiency of approximately 20% at the standard deuterium target location (7406 mm downstream of the radiator). We will measure the tagging efficiency throughout the experiment on a daily basis using

[4] Note that after the Nov08 runperiod, the SAL focal plane will most likely be re-instrumented with brand new scintillator. Further, at the time of this writing, the Lund Group has been awarded an MRI from the Wallenberg Foundation to build a next-generation focal plane. The details of this focal plane are not important to this proposal, but the projected photon-energy resolution over the applicable energy range will be 250 keV rather than 650 keV, the value used throughout the remainder of this proposal. This focal plane may also be available for production running.

the standard, low-intensity invasive technique. We will monitor the tagging efficiency continuously throughout the experiment using the non-invasive IBM technique [17]. We employ the standard value of 4×10^5 MeV^{-1} s^{-1} for the photon flux (which has been scaled for the contribution of the tagging efficiency) for the remainder of the proposal.

2.2.2 Target

We intend to employ the MAX-lab liquid deuterium target [18–22] (originally from Göttingen, Germany) which is fully functional and routinely employed during the Compton program. The largest possible target cell presently available is 68 mm in diameter by 150 mm in length. The symmetry axis of this cell lies along the photon-beam axis. See Fig. 5.

Fig. 5. The liquid deuterium target cell. The cell is 68 mm in diameter by 150 mm in length. The symmetry axis of the cell lies along the photon-beam axis.

We employ a value of 0.162 g cm^{-3} for the density of liquid deuterium. This translates to an areal density of 3.63×10^{23} cm^{-2} for the 150 mm target cell. We employ the value

3.63×10^{23} cm^{-2} for the remainder of the proposal.

We have access to a dummy target produced by the COMPTON@MAX-lab Collaboration which consists of 200 sheets of the Kapton used for the target cell. This dummy target will allow us to perform the empty-target measurements in an efficient fashion. We do not anticipate a large background from the target cell; nevertheless, we plan to perform dedicated measurements of this background on a regular basis.

2.2.3 Photon detectors

Inhouse and fully operational at MAX-lab, we have three of the largest single-crystal NaI(Tl) spectrometers ever built – CATS [23] (on loan from the University of Mainz, Germany – see Fig. 6), BUNI [24] (on loan from Boston University, USA), and DIANA [25] (on loan from the University of Kentucky, USA).

Fig. 6. The CATS detector (on loan from the University of Mainz, Germany) shown *in situ* at MAX-lab. The detector itself is encased in lead shielding, and the resulting canister is mounted on a heavy steel frame. The steel frame sits on airpads which allows for the entire apparatus to be postioned with relative ease. The other two detectors are very similar.

Each of these detectors boasts an energy resolution of at least 2% for 100 MeV photons, which is more than adequate for the intended measurements of the photon channel. GEANT4 simulations by our COMPTON@MAX-lab colleagues have demonstrated that at 130 MeV, the NaIs detect 95% (99%) of the incident photons with 90% (80%) or

more of their incident energy using only the core. When the quads are included, the NaIs detect 96% (99%) of the incident photons with 95% (90%) or more of their incident energy [26].

The detectors will be placed at angles of 60° beam right, 150° beam right, and 120° beam left. Experience gained during the Compton program has demonstrated that the large NaIs cannot handles the rates associated with the full deuterium target forward of 60°, and that there must be an angular offset of 90° between detectors in order to maximize the solid angle they subtend. The third angle, 120° beam left, has been chosen so that the beam left quadrant from 0° to 90° is free from obstructions. We will position our neutron detectors (see Sect. 2.2.4) in this region. The measurement of the cross section with three different detectors at three different angles will allow us to better understand our systematics.

We employ a value of 40 msr for the solid angle subtended by a photon detector and 98% for the detection efficiency for a photon detector for the remainder of this proposal.

2.2.4 Neutron detectors

In addition to the three large NaI detectors previously discussed (see Sect. 2.2.3), we intend to simultaneously use one of the following two types of neutron detectors. An independent measurement of the cross section via the neutron channel will allow us to better understand our systematics.

Lund TOF array

In house at MAX-lab, we have the Lund plastic-scintillator neutron array. This array consists of 10 bars that are $300 \times 20 \times 10$ cm^3. Each bar is instrumented with tubes and bases at either end. We will place the resulting $300 \times 200 \times 10$ cm^3 wall at 40° beam left and a distance of 3 m from the target to measure the 68 MeV neutrons from the neutron channel. We thus anticipate a solid angle of 670 msr and a detection efficiency of ∼10%. However, as neutron time-of-flight measurements have not yet been attempted at the upgraded facility with the new electron beam and its associated time structure, some testing will first need to be performed. That said, given the monoenergetic 68 MeV neutron, we are cautiously optimistic [5].

NORDBALL PSD array

Should conditions for neutron detection via TOF prove unfavorable, we will instead employ a segmented liquid-scintillator array. In house at MAX-lab, we have at least 16 elements of the NORDBALL [20,27]. These detectors allow for the detection and

[5] Note that Annand *et al.* intend to use this array for their near-threshold photodisintegration of ^{4}He measurement. We intend to work closely with them in developing and testing the detector.

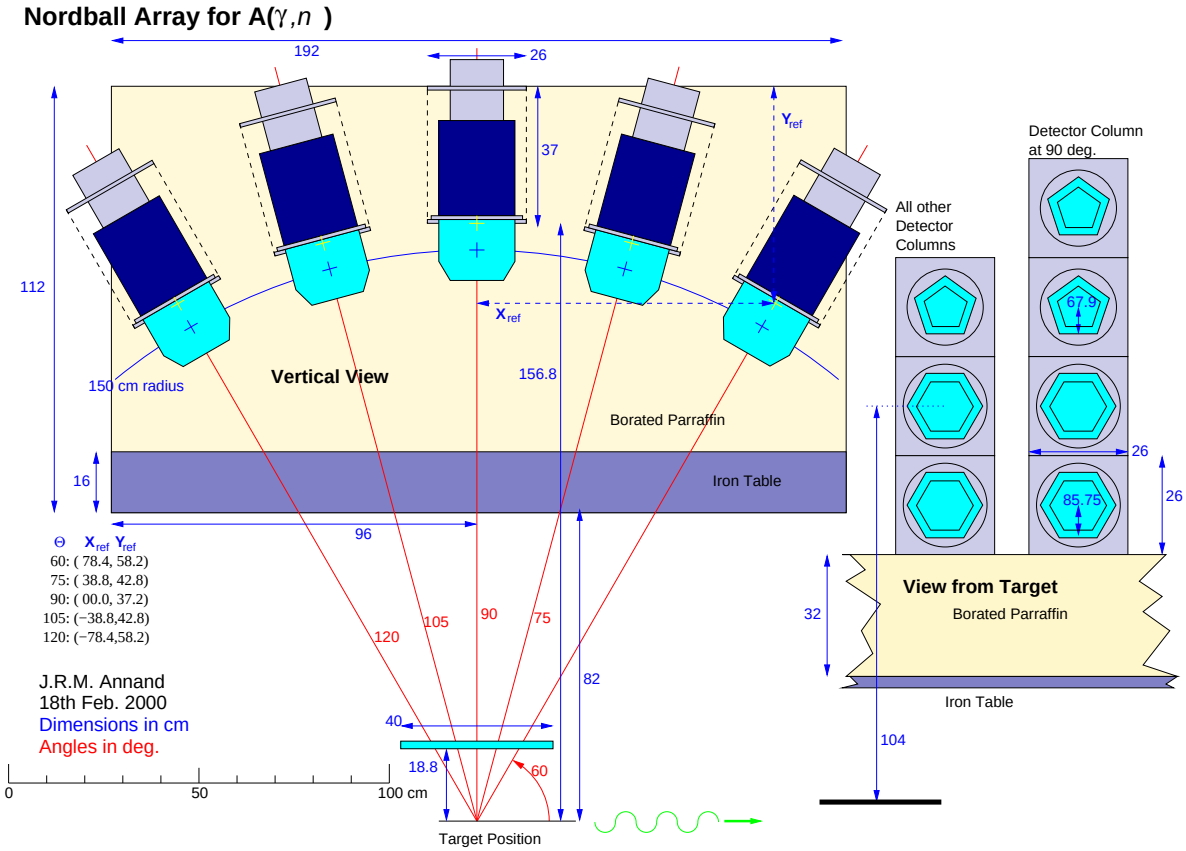

Fig. 7. An overview of a previously used NORDBALL geometry. Note the plastic-scintillator charged-particle veto detector near the target.

identification of neutrons via pulse-shape discrimination. We will use these detectors in a 4 × 4 configuration at an angle of 40° beam left and a distance of 1 m from the target to measure the 68 MeV neutrons from the neutron channel (see Fig. 7). We thus anticipate a solid angle of 545 msr and a detection efficiency of ∼10%. As neutron PSD measurements have not yet been successfully performed at the upgraded facility with the new electron beam and its associated backgrounds, some testing will first need to be performed. That said, given the conservative placement of the PSD array, we are again cautiously optimistic [6] .

Since we intend to use the measurement of the neutron channel to complement our measurement of the photon channel, we do not base our beamtime request upon the characteristics of the neutron detectors.

[6] Note that Annand *et al.* intend to use this array for their near-threshold photodisintegration of ^{4}He measurement. They have pledged to replace the aging liquid scintillator in the NORDBALL detector elements so that the array will be in peak condition for these measurements. We intend to work closely with them in revamping and testing the detector.

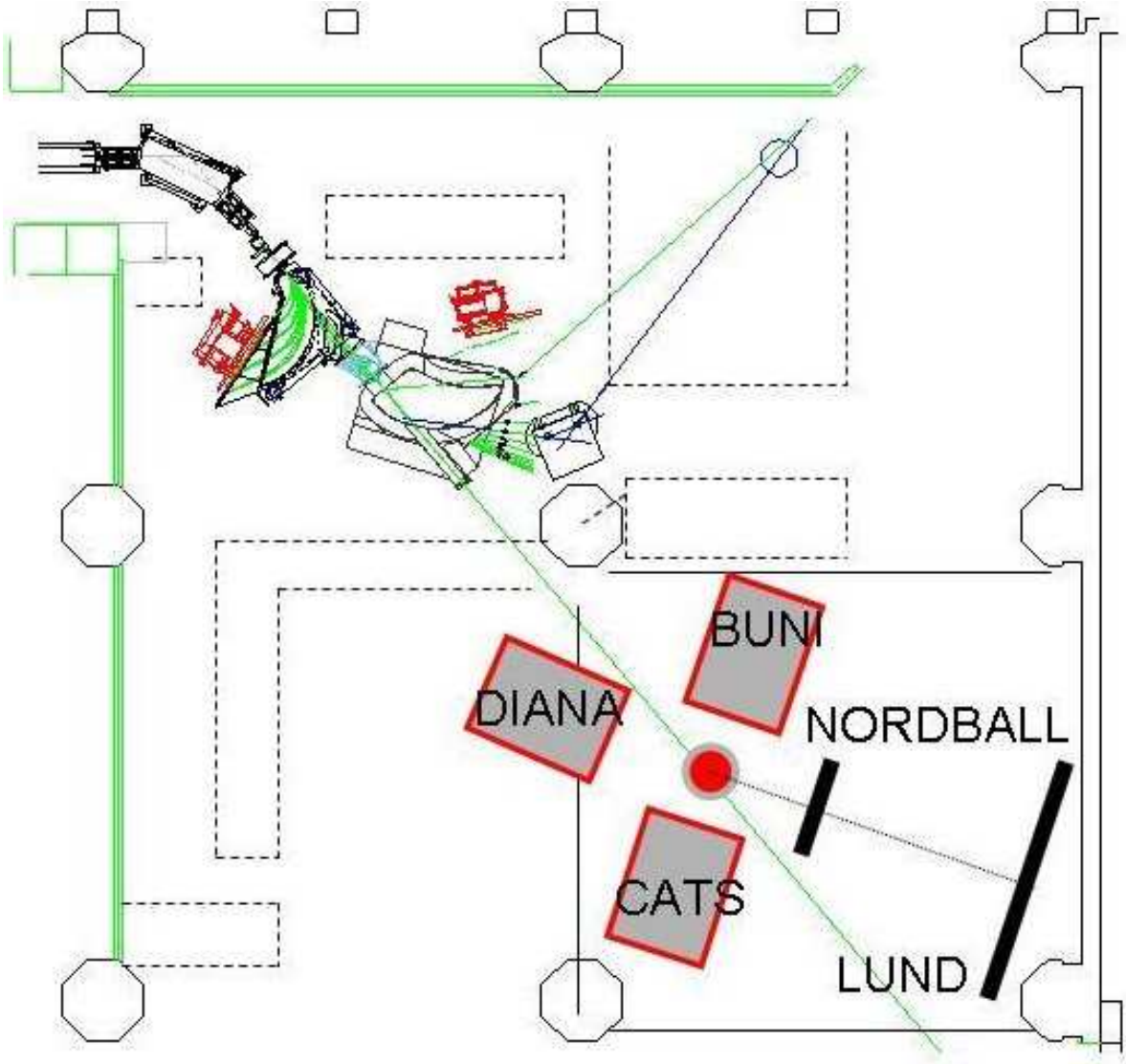

Fig. 8. An overview of the experimental setup (not to scale). Together with the liquid deuterium target, the three large NaI detectors are shown at 60° beam right (CATS), 150° beam right (DIANA), and 120° beam left (CATS). Also shown are neutron detectors at 40° beam left – either the NORDBALL PSD array at a distance of 1 m or the LUND TOF array at a distance of 3 m.

2.2.5 Data-acquisition system

We intend to use the DAQ in the large data-acquisition room which has already been configured for production running of the large NaIs and tagger by the COMPTON@MAX-lab Collaboration, and thus will only need minor adjustments for the proposed experiment. One such adjustment will be the addition of multi-hit TDCs to the tagger focal-plane instrumentation, which will in principle allow for the elimination of the "stolen-coincidences" correction to the data. At the time of this writing, all the necessary electronics, including PSD modules, NIM bins, and CAMAC and VME crates, are already in house.

We employ a data-acquisition livetime efficiency of 50% for the remainder of this proposal.

2.3 Rate estimate

2.3.1 Base calculation per detector per tagger channel

We base our π^- rate estimate for a single NaI detector for a single focal-plane channel on the following expression:

$$\dot{N}_{\pi^-}(E_\gamma,\theta) = \overline{\frac{d\sigma}{d\Omega}}(E_\gamma,\theta)\cdot\Delta\Omega\cdot t'\cdot\dot{N}_\gamma\cdot\Delta E_\gamma\cdot\varepsilon_{\rm live}\cdot R\cdot C_{\pi^-}\cdot A_{\pi^-}\cdot\varepsilon_\gamma, \qquad (1)$$

where $\dot{N}_{\pi^-}(E_\gamma,\theta)$ is the π^- rate, $\overline{d\sigma/d\Omega}(E_\gamma,\theta)$ is the average differential cross section, $\Delta\Omega$ is the average detector solid angle, t' is the areal density of photoproduction centers in the target, $\dot{N}_\gamma$ is the photon flux, ΔE_γ is the width of a single tagger channel in photon-energy space, $\varepsilon_{\rm live}$ is the data-acquisition livetime efficiency, R is the π^--capture branching ratio, C_{π^-} is the containment efficiency (see Sect. 2.3.2), A_{π^-} is the attentuation of π^-s due to nuclear interactions in the target (see Sect. 2.3.3), and ε_γ is the capture-photon detection efficiency. We summarize these parameters in Table 5. We evaluate our rate-estimate expression only for the measurement of the photon channel, and base our beamtime request upon this rate estimate. This is because we consider our measurement of the neutron channel to be complementary.

Quantity	value
$< d\sigma/d\Omega >$	1 μb/sr
$\Delta\Omega$	40 msr
t'	3.63×10^{23} cm^{-2}
N_γ	4×10^5 MeV^{-1} sec^{-1}
ΔE_γ	650 keV
$\varepsilon_{\rm live}$	0.50
R	0.25
C_{π^-}	1.00
A_{π^-}	0.90
ε_γ	0.98

Table 5
A summary of the anticipated experiment parameters folded into our per tagger channel π^- rate estimate for a single NaI detector.

Our anticipated π^- rate per tagger channel per NaI detector is thus 1.5 per hour. This results in 181 π^- per tagger channel per NaI detector per nominal beam week, which means a measurement to the level of 3.7% statistics for the first eight [7] 650 keV photon-energy bins spanning the energy range from 146 to 151 MeV (the s-wave region [8] for each detector will require about 480 hours of beamtime corresponding to four nominal beam weeks. The data from the three detectors will then be combined, resulting in a measurement to the level of 2.1% statistics.

2.3.2 On the containment efficiency

The "containment efficiency" is the term we use to describe the fact that any given π^- must first be stopped in the liquid deuterium target in order for it to be captured and the reaction products of the capture be detected. For the purposes of our rate estimate in the previous section, we employed a value of unity for this parameter, which implies that no π^-s escape the target volume without capturing. Clearly, this is a critical parameter. To first order, it depends on several variables: the photon-beam spot size and thus the photon-beam collimator, the tagged-photon energy range and thus the tagged-pion energy range, and the dimensions of the target canister (both radial and longitudnal), and thus the energyloss of the π^-s in the target. While our target size is fixed at 68 mm diameter $\times$ 150 mm in length and our tagged-photon energy range is fixed at 146 – 167 MeV, our photon-beam collimator size has yet to be optimized. The choice of the size of the photon-beam collimator is driven by maximizing the tagging efficiency (which requires the largest possible collimator that still ensures that the photon-beam spot size is completely subtended by the target volume) while at the same time ensuring that the π^-s produced away from the center of the beamspot do not have sufficient energy to escape. Clearly, this parameter will require a substantial simulation to establish, and at the time of the writing of this proposal, our simulations group has not progressed to this point. Thus, in the meantime, we have addressed the issue "by hand".

We define the photon-energy region critical to this experiment to be that subtended by the first 12 focal-plane channels, where the reaction is "reasonably" s-wave. Four of these channels are sub-threshold. The highest photon energy corresponding to this critical region is thus 151 MeV. Photons of this energy produce π^-s with energies ranging from 6.5 MeV at 0° to 50 keV at 180°. Backward of 90°, π^-s have less than 1 MeV energy.

Clearly, in this simple, geometrical model, π^-s produced at a 90° angle on the perimeter of the photon beam see the least liquid deuterium. A 1 MeV π^- has a range of about

[7] Note that four of these channels will be "empty" as they are sub-threshold. Including sub-threshold data in our measurement will aid in the interpretation of our systematics.

[8] Data corresponding to the tagger channels from 151 to 167 MeV will also be acquired, potentially at a much higher rate (depending upon the containment efficiency – see Sect. 2.3.2). These data will clearly include substantial p-wave contributions. While we have constructed the experiment about the s-wave measurement, these data come for "free".

1 mm. This would suggest that we should employ a photon-beam collimator which resulted in a 66 mm diameter photon-beam spot. However, as we go forward in angle, while the amount of liquid deuterium seen by the π^- increases, so does the energy. At 45°, the energy has increased to 3.7 MeV and the range to 1 cm, so that a photon-beam collimator which results in a 54 mm photon-beam spot is necessary to ensure that the π^- in question sees enough deuterium to prevent it from escaping. At 30° (where the combination of π^- energy and deuterium thickness seems its worst), the energy has increased to 5.1 MeV and the range to 1.7 cm, so that a photon-beam collimator which results in a 50 mm photon-beam spot is necessary. Our COMPTON@MAX-lab colleagues report that this will require a photon-beam collimator of diameter 25 mm, which will result in a tagging efficiency of about 20% [26].

Thus, we will employ a photon-beam collimator that ensures all π^-s corresponding to the first 12 tagger channels will stop in the target. We intend to simulate the containment correction for the higher-energy channels.

2.3.3 On the yield attenuation due to π^- interactions other than capture

Interactions between the photoproduced π^-s and the target deuterium (πD interactions) other than the desired capture reaction can significantly attenuate the measured yield. πD interactions include multiple small-angle Coulomb scattering, single large-angle Coulomb and nuclear scattering, inelastic scattering, and charge exchange.

Multiple small-angle Coulomb scattering involves the π^- undergoing a large number of scatterings from the target atoms. Single large-angle scattering is due to both Coulomb scattering from the nuclear charge and nuclear scattering from the nucleons. Elastic scattering can cause the π^- to scatter out of the target volume and go undetected. Inelastic scattering involves the π^- being degraded in energy by exciting a target deuteron and scattering through some angle. The charge-exchange interaction involves the charge conversion of the π^-.

Again, as our simulation group is not yet up and running, we have been unable to thoroughly investigate these phenomena. However, based upon experience with the π^+ channel [28] together with a literature survey for the π^- channel, we have assigned a very conservative yield loss of 10%. We intend to simulate the yield attenuation due to π^- interactions other than capture.

2.3.4 On the π^0 background

We identify the competing π^0 photoproduction mechanism as our greatest source of background. π^0s may be produced from the proton, from the neutron, as well as coherently from the deuteron.

For the case of the proton and the neutron, the total π^0 photoproduction cross section

at the highest tagged-photon energy is approximately 5 μb, while the total photoproduction cross section for the $\gamma + n \rightarrow p + \pi^-$ reaction is approximately 100 μb. For the case of coherent π^0 production from the deuteron, we suppose a simple A^2 dependence, so that the coherent photoproduction cross section will be approximately 20 μb. Furthermore, kinematics are such that coherent π^0s always have about 2 MeV more energy. We thus address this as the dominant mechanism for the production of competing background.

Figure 9 shows the kinematic relation between the π^0 decay-photon energies and the opening angle between the decay photons for coherent photoproduction on deuterium. The top panel corresponds to 167 MeV tagged photons (our maximum energy), while the bottom panel corresponds to 148 MeV tagged photons (our minimum energy). In both cases, the filled circles correspond to the most energetic possible π^0s (those produced at 0° with respect to the direction of the photon beam), while the open squares correspond to the least energetic possible π^0s (those produced at 180° with respect to the photon beam). For 167 MeV photons, the most energetic π^0s have 30.7 MeV, while the least energetic have 17.1 MeV. For 148 MeV photons, the most energetic π^0s have 10.7 MeV, while the least energetic have 4.2 MeV. The curve for π^0s produced at 90° with respect to the direction of the photon beam will thus lie between these two extreme curves. The horizontal line labeled "cutoff" positioned at 100 MeV photon energy is taken from the base width of the gamma-ray peak shown in Fig. 3. We believe that any π^0 decay-photon phase space lying below this cutoff will not affect our experiment.

For the special case of the minimum opening angle between the two decay photons, each photon receives half of the energy of the π^0. As the opening angle increases, the decay photons begin to share the energy disproportionately. Further, as the opening angles increases, the direction of the most energetic photon rotates towards the direction of the original π^0 and the direction of the least energetic photon rotates away from the direction of the original π^0. The extreme case occurs when the opening angle is 180° – in this case, the most energetic photon travels in the direction of the original π^0.

Data [29,30] show that the coherent π^0 angular distributions vary from strongly backward peaked at 142 MeV to slightly forward peaked by 172 MeV. The most probable π^0 angle will thus be backward of 90° with respect to the direction of the photon beam. Hence, we see very clearly that each of our detectors will potentially be subjected to a photon background resulting from the decay of π^0s.

Figure 10 shows the relative probability for a decay photon of a given energy for our most challenging photon energy of 167 MeV. The upper panel corresponds to 30.7 MeV π^0s (those produced at 180° with respect to the photon beam), while the bottom panel corresponds to 17.1 MeV π^0s (those produced at 180° with respect to the photon beam). The vertical line labeled "cutoff" positioned at 100 MeV photon energy is again taken from the base width of the gamma-ray peak shown in Fig. 3. By comparing the top panel of Fig. 9 to this figure, one can clearly see that while the phase-space volume above 100 MeV is indeed accessible to the π^0 decay photons, the relative probability

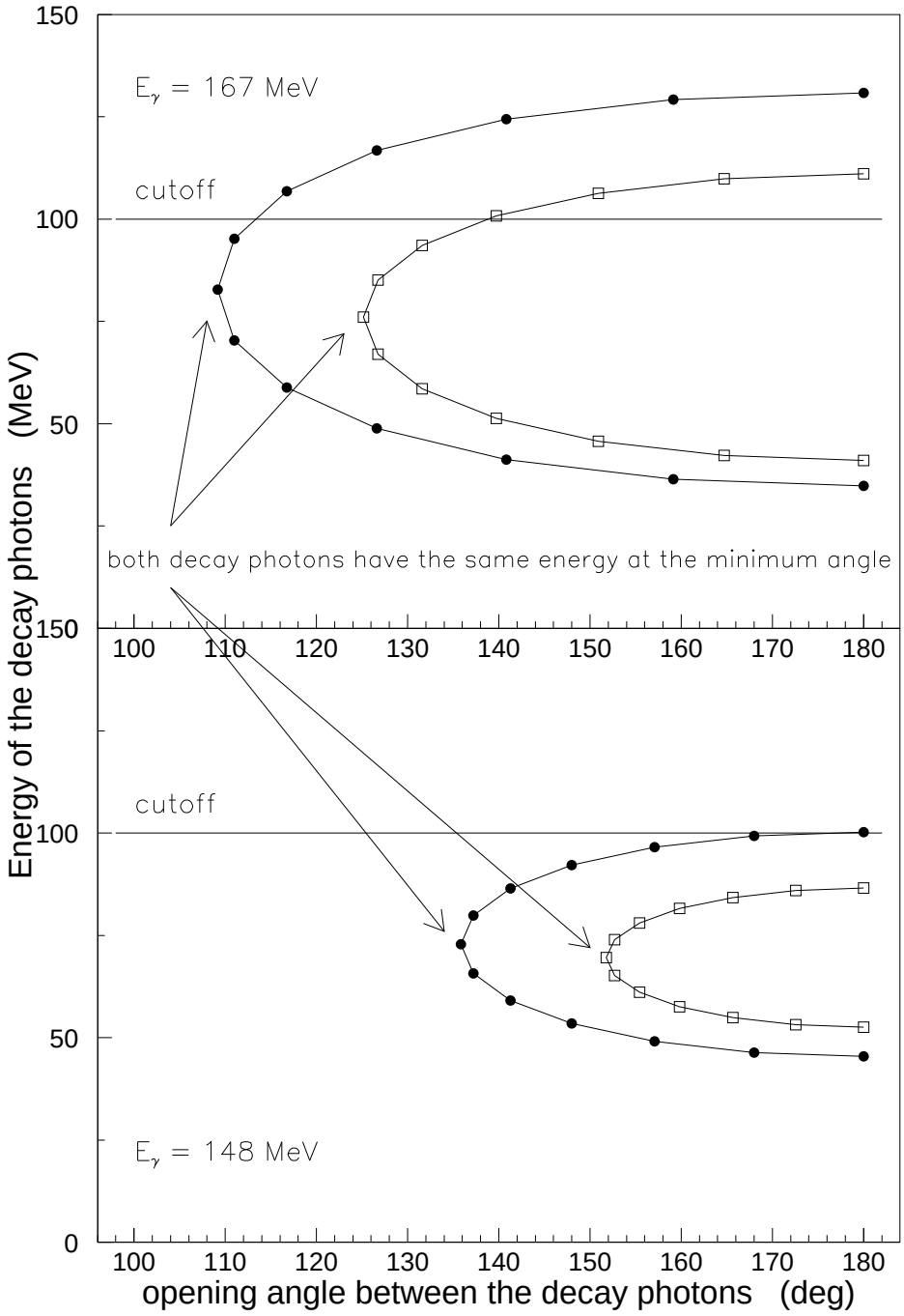

Fig. 9. The kinematic relation between π^0 decay-photon energies and the opening angle between the decay photons for coherent photoproduction on deuterium. In each panel, the filled circles correspond to the most energetic π^0s (those produced at 0° with respect to the direction of the photon beam), while the open squares correspond to the least energetic π^0s (those produced at 180° with respect to the photon beam). The horizontal line labeled "cutoff" positioned at 100 MeV photon energy is taken from the base width of the gamma-ray peak shown in Fig. 3. See text for further details.

for populating it is rather small.

Energetics and phase-space arguments imply that the s-wave region measurement about which the entire experiment is optimized will be subjected to the smallest π^0 decay-photon background. Our sub-π^- threshold tagger channels will in fact enable us to measure only this background. We anticipate that this will help. Even in our worst-case kinematics, the population of the phase-space volume element in question is relatively small. The fact that we have three photon detectors positioned at three different angles should allow us to unfold the background as a function of angle for each photon-energy bin. We anticipate that this will also help. Together with our simultaneous measurement of the neutron channel and our planned extensive modeling of the experiment (see Sect. 2.4), we conclude that the π^0 background we shall see in this experiment should be manageable.

2.4 Experiment simulation and data analysis

One may argue that in the case of π^- photoproduction, with results which must be extracted from a "two-step" measurement, performing the experiment may in fact be simpler than the analysis and interpretation of the data. This is because the extraction of the amplitudes is complicated by the bound-state momentum distribution of the neutron and final-state interactions. We do not argue this point – this is a challenging experiment.

In order to facilitate this process, our "simulations group" has purchased several powerful PCs for the purpose of modeling this experiment in detail before the actual run, as well as aiding in the data analysis once the data are taken. At the time of this writing, GEANT4 and ROOT have been loaded onto the simulation machines, compiled, and are fully functioning. Additionally, on a subset of the machines, the event generator is working. Further, models of the three large NaI detectors and the deuterium target have been acquired from the COMPTON@MAX-lab Collaboration. A base Monte Carlo for this experiment is thus already in place, and the next step will be to create controlled input to test its functionality and make sure that all the necessary virtual data for the optimization of the experiment is being created. The anticipated time of completion for this project is 1 November 2008.

2.5 Systematic uncertainties

Given the fact that we will be inheriting a well-studied, calibrated, and commissioned apparatus, we anticipate no difficulties associated with performing the experiment itself, and thus with confidence quote the 5% systematic uncertainty associated with the mechanics of the measurement given to us by our COMPTON@MAX-lab colleagues.

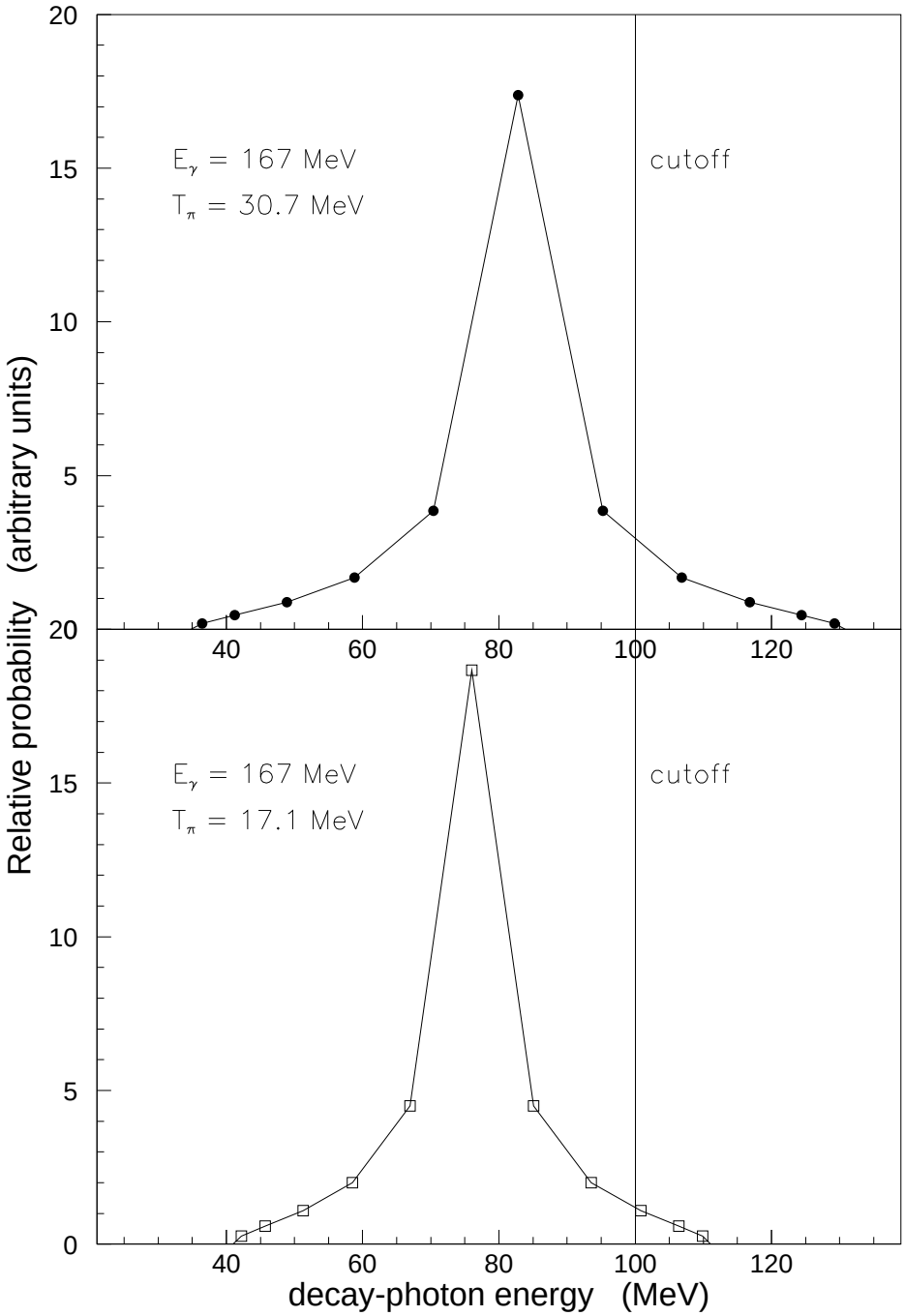

Fig. 10. The relative probability for π^0 decay-photon energies at $E_\gamma = 167$ MeV (the worst-case scenario). The filled circles in the top panel correspond to 30.7 MeV π^0s produced at 0° with respect to the direction of the photon beam, while the open squares correspond to 17.1 MeV π^0s produced at 180° with respect to the photon beam. The vertical line labeled "cutoff" positioned at 100 MeV photon energy is again taken from the base width of the gamma-ray peak shown in Fig. 3. The relative probability for populating the phase-space volume above 100 MeV is small. See text for further details.

Quantity	beam hours
reconfigure NaIs and commission	120 hours
setup and commission neutron detectors	240 hours
target overhead (filling and cooling)	30 hours
empty-target measurements	30 hours
tagging-efficiency measurements	60 hours
detector calibrations (sources, in-beam)	120 hours
production	480 hours

Table 6
An overview of our beamtime request for this experiment.

That said, we anticipate that the interpretation of the data may not be as straightforward as we would like, given the nature of the measurement. As previously discussed, we expect to rely heavily on stringent modeling of our experiment in our interpreation of the results. We thus assign another anticipated 5% systematic uncertainty to our unfolding of the results, for a total anticipated systematic uncertainty of 7.1%.

3 Beamtime request

We request 120 hours of beamtime (one nominal beam week) for the reconfiguration, setup, and shakedown of the NaI detectors from their present "Compton scattering" mode to the new "detection of photons from π^- capture" mode. We request 240 hours of beamtime (two nominal beam weeks) for the setup, calibration, and commissioning of the NORDBALL PSD array elements together with the LUND TOF array elements. As has been shown, 480 hours of beam on target is sufficient to make a 2.1% statistical measurement for the photon channel. To round things out, we request 240 hours of beamtime (two nominal beam weeks) for typical experiment overhead such as associated target work, detector calibrations, and tagging-efficency measurements.

We thus request a total of 9 nominal beam weeks.

Figure 11 shows the antipated data set superimposed upon the existing data already presented in Fig. 2. The FA07 result is shown by the solid blue line, while the MAID07 result is shown by the dot-dashed magneta line. Also shown is our projected total uncertainty shown by the error bar on the black data point. This error bar represents the quadratic sum of our projected 2.1% statistical uncertainty together with our anticipated 7.1% systematic uncertainty.

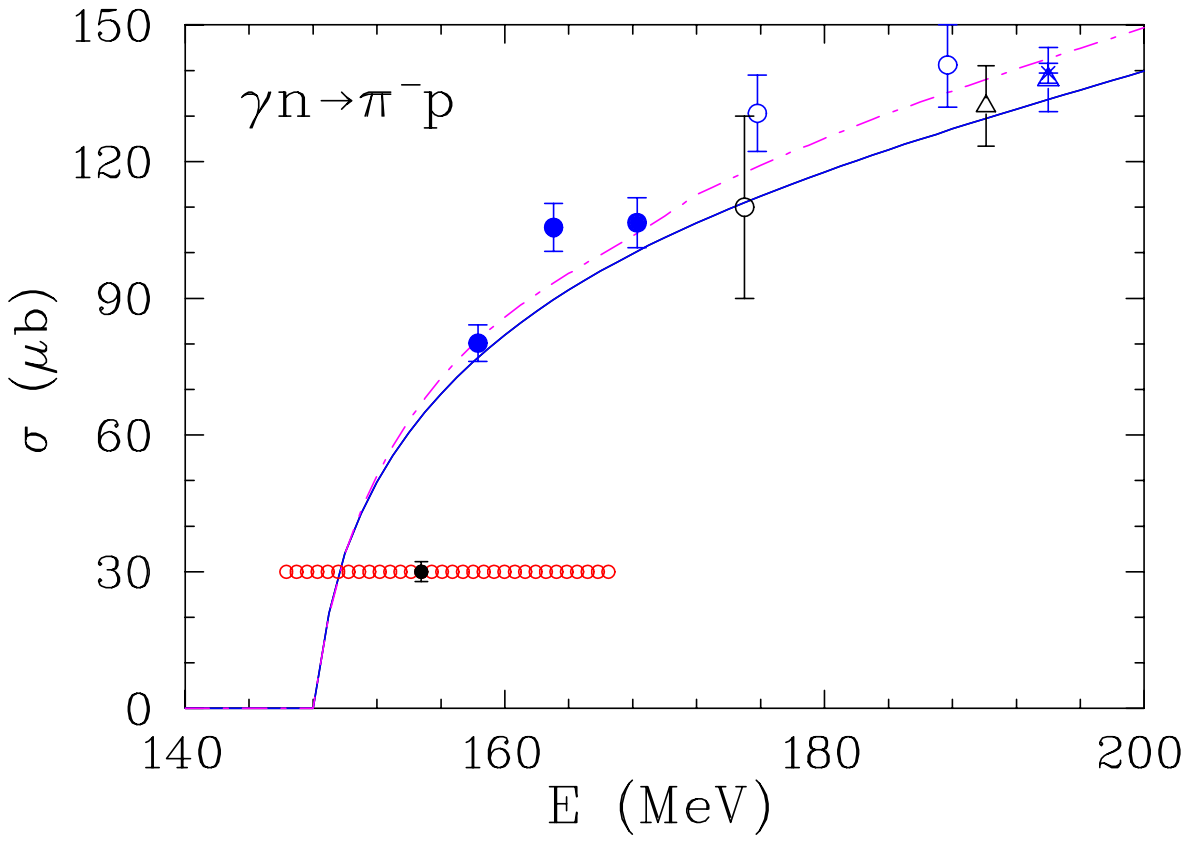

Fig. 11. The anticipated data set superimposed upon the existing total cross-section data for the $\gamma + n \rightarrow p + \pi^-$ reaction as a function of photon energy (recall Fig. 2). The FA07 result is shown by the solid blue line, while the MAID07 result is shown by the dot-dashed magneta line. The error bar associated with the black data point is representative of our projected uncertainties.

4 Summary

The determination of the resonance properties of nucleon states is one of the primary goals of nuclear physicists. Pole positions, decay channels, magnetic moments, and electromagnetic couplings provide a crucial body of information which may be used to test QCD-inspired models of the nucleon, and more recently, lattice-QCD calculations.

The determination of neutron couplings is a critical issue within the nucleon-resonance program. Most of the sparse photoneutron data available have originated in experiments performed at bremsstrahlung faiclities and have large (and often unreported) systematic uncertainties. The only "available" data anywhere near our region of interest have been measured using the inverse reaction and remain preliminary. To our knowledge, no data measured using the forward reaction have been taken in the threshold energy region.

In order to be effective, models such as MAID and model-independent technologies such as SAID require comparable proton and neutron databases. At the moment, such databases do not exist. We have thus optimized our experiment for the *s*-wave region

to fully complement the data of Ref. [6]. Further, while the sensitivity is not as great as for the uncharged channels, this s-wave region is clearly of particular interest for comparisons between LETs and ChPT, and we anticipate that a new precision data set in a never-before investigated energy region will be welcomed. Finally, we anticipate that our total cross-section data will extend well into the p-wave region, which is now accessible to ChPT theorists [31–37]. While obviously not as desirable as data differential in angle, it will certainly be useful to establish the baseline for future measurements.

References

[1] G. Ecker *et al.*, Comm. Nucl. Part. Phys. **21**, 347 (1995).

[2] V. Bernard, N. Kaiser, and U.-G. Meißner, Phys. Lett. B. **383**, 116 (1996).

[3] for example, D. Drechsel *et al.*, Eur. Phys. J. A **34**, 69 (2007); see also `http://www.kph.uni-mainz.de/MAID/maid.html`

[4] for example, M. Dugger *et al.*, Phys. Rev. C **76**, 025211 (2007) – this is SP06. For FA07, recent SPring-8 $\pi^0 p$ data and preliminary CLAS $\pi^+ n$ (ASU analysis) and $\pi^- p$ (Duke analysis) have been included; see also `http://gwdac.phys.gwu.edu/`

[5] The full database and numerous PWAs with potential models may be accessed via an *ssh* call to the SAID facility `gwdac.phys.gwu.edu` with userid: said (no password), or a visit to the website: `http://gwdac.phys.gwu.edu`.

[6] E. Korkmaz *et al.*, Phys. Rev. Lett. **83**, 3609 (1999).

[7] M. Kovash for E643, PiN Newsletter **12N3**, 51 (1997); see also M.A. Kovash in *Chiral Dynamics: Theory and Experiment*, edited by A.M. Bernstein and B.R. Holstein (Springer Lecture Notes in Physics, Heidelberg, 1995).

[8] H. Greisshammer, private communication (2006).

[9] N.M. Kroll *et al.*, Phys. Rev. **93**, 233 (1954).

[10] R. Koch, Nucl. Phys. **A448**, 707 (1986).

[11] R. Arndt *et al.*, Phys. Rev. C **74**, 045205 (2006).

[12] J.P. Burg, Ann. Phys. **10**, 363 (1965).

[13] E.L. Goldwasser *et al.*, *Proc. XXII Int. Conf. on High-Eenrgy Physics, Dubna, 1964*, edited by Ya. A. Smorodinsky (Atomisdat, Moscow, 1966).

[14] SAL051 Status, Saskatchewan Accelerator Laboratory Annual Report 83 (1994).

[15] `http://www.maxlab.lu.se/kfoto/UserInfo/ETenergies2008rev.doc`

[16] J. M. Vogt *et al.*, Nucl. Instrum. Methods **A324**, 198 (1993).

[17] `http://www.maxlab.lu.se/kfoto/ExperimentalProgram/np006/apparatus/diverse/ibms/figsphotos/IBM.20.09.07.pdf`

[18] T. Glebe, Diplomarbeit, II. Physikalischen Institut der Georg-August Universität zu Göttingen, unpublished (1993).

[19] M. Lundin, PhD Thesis, Lund University, unpublished (2002).

[20] `http://www.maxlab.lu.se/kfoto/ExperimentalProgram/np014/physics/loi05.pdf`

[21] `http://www.maxlab.lu.se/kfoto/ExperimentalProgram/np006/apparatus/target/target.html`

[22] http://www.maxlab.lu.se/kfoto/ExperimentalProgram/runperiods/runperiod13.pdf

[23] http://www.maxlab.lu.se/kfoto/ExperimentalProgram/np006/apparatus/detectors/cats/cats.html

[24] http://www.maxlab.lu.se/kfoto/ExperimentalProgram/np006/apparatus/detectors/buni/buni.html

[25] http://www.maxlab.lu.se/kfoto/ExperimentalProgram/np006/apparatus/detectors/diana/diana.html

[26] L. Myers, private communication (2008).

[27] A. Reiter *et al.*, Nucl. Instrum. Methods **A565**, 753 (2006).

[28] K. Fissum, PhD Thesis, University of Saskatchewan, unpublished (1993).

[29] J. C. Bergstrom *et al.*, Phys. Rev. C **57**, 3203 (1998).

[30] U. Siodlaczek *et al.*, Eur. Phys. J. A **10**, 365 (2001).

[31] N. Fettes *et al.*, Nucl. Phys. **A640**, 199 (1998).

[32] P. Buettiker *et al.*, Nucl. Phys. **A688**, 97 (2000).

[33] H. W. Fearing *et al.*, Phys. Rev. C **62**, 054006 (2000).

[34] N. Fettes *et al.*, Nucl. Phys. **A679**, 629 (2001).

[35] T. Hemmert arXiv:nucl-th0209067 (2002).

[36] M. C. M. Rentmeester *et al.*, Phys. Rev. C **67**, 044001 (2003).

[37] E. Epelbaum *et al.*, Nucl. Phys. **A747**, 362 (2005).

[38] O. Hanstein *et al.*, Nucl. Phys. **A632**, 561 (1997).